# In-situ observation of pre-, co- and post-seismic shear slip at 1.5 km depth

Martin Schoenball, Yves Guglielmi, Jonathan B. Ajo-Franklin, Paul Cook, Patrick F. Dobson, Chet Hopp, Timothy J. Kneafsey, Florian Soom, Craig Ulrich and EGS Collab Team

## Key points:

- Direct observation of displacement from a shear rupture in crystalline rock at 1.5km depth
- Rupture was observed including transients of aseismic pre-slip, co-seismic, and afterslip phases
- Co-seismic rupture phase accounts for only 25% of total slip

## Abstract

Understanding the initiation and arrest of earthquakes is one of the long-standing challenges of seismology. Here we report on direct observations of borehole displacement by a meter-sized shear rupture induced by pressurization of metamorphic rock at 1.5 km depth. We observed the acceleration of sliding, followed by fast co-seismic slip and a transient afterslip phase. Total displacements were about 7, 5.5 and 9.5 micrometers, respectively for the observed pre-slip, co-seismic slip and afterslip. The observed pre-slip lasted about 0.4 seconds. Co-seismic slip was recorded by the 1 kHz displacement recording and a 12-component array of 3-C accelerometers sampled at 100 kHz. The observed afterslip is consistent with analytical models of arrest in a velocity-strengthening region and subsequent stress relaxation.

The observed slip vector agrees with the activation of a bedding plane within the phyllite, which is corroborated by relocated seismic events that were observed during the later stages of the injection experiment.

## Plane language summary

Because earthquakes typically occur at great depths, and we cannot predict when and where the next event will occur, it is very difficult to observe their beginning and their end. We instrumented a borehole in a 1.5 km deep mine with precise displacement sensors and created a meter-sized rupture through fluid injection. We were not only able to capture the fast displacement that is responsible for the ground

shaking associated with earthquakes, but also its slow onset and finally the decelerating until its arrest. From our measurements we inferred that only about a quarter of the total displacements is associated with seismic waves, while most of the displacement is slow. Further analysis revealed that the event aligned with bedding planes of the host rock and not – as commonly assumed – with natural fractures.

## Introduction

How do earthquakes start? This is a fundamental question that to date has not been answered by direct observational data. Knowing how earthquakes initiate could have important implications on rapid assessment of earthquakes with applications to earthquake early warning. Capturing the onset of an earthquake with sensors close to the hypocenter could provide important insights towards furthering our understanding of rupture initiation. However, not knowing when and where the next earthquake occurs almost precludes efforts to capture the initiation of a tectonic earthquake with direct measurements. Further, the depth of most earthquake hypocenters prohibits instrumenting even known repeating earthquake hypocenters with in-situ sensors (Nadeau & Johnson, 1998; McGuire et al., 2005; Savage et al., 2017).

Two endmember models exist that describe the onset of earthquakes and are debated in the community. The first, the cascade model (Ellsworth & Beroza, 1995), is based on small ruptures coalescing into a larger rupture promoted by static stress transfer. Prominent examples are observations of foreshock sequences observed for the 1999 Hector Mine (Yoon et al., 2019) and Izmit (Ellsworth & Bulut, 2019) earthquakes. The complementary model, the pre-slip model, argues for stable-sliding pre-slip transitioning into slip-weakening behavior and reaching seismic slip speeds accompanied by seismic wave radiation and ground shaking. While this model has significant theoretical support from dynamic rupture modelling (Cattania & Segall, 2020 and references therein) observational support for this model is sparse. Rare examples include the observation of very low frequency events accelerating into earthquakes in Alaska (Tape et al., 2018) and laboratory experiments on meter-sized samples (McLaskey & Lockner, 2014; McLaskey, 2019).

Here we present direct observations in support of the pre-slip model from a series of meso-scale injection experiments performed at 1480 m depth. Using passive seismic monitoring and in-situ displacement sensors sensitive to µm-scale deformation and rotation we closely tracked the initiation of a hydraulic fracture, i.e., an opening mode fracture that propagates for pore fluid pressures greater than the least principal stress (Guglielmi et al., 2021). During the pressurization stage, and before the initiation of the hydraulic fracture, we observed the slippage caused by a single shear event including its pre-slip, co-

seismic and afterslip phases. Subsequently, we will provide a brief overview of the setup of the injection experiment and in-situ observations of hydraulic fracturing. We then focus on the shear event and its pre-seismic, co-seismic and post-seismic phases.

## Experimental setup and data

The EGS Collab project (Kneafsey et al., 2019; 2020; 2021) experimental testbeds are located in the Sanford Underground Research Facility in Lead, South Dakota, which provides easy access to rock with 1.5 km of overburden (Heise, 2015). We established a testbed in a metamorphic rock mass comprising six dedicated monitoring boreholes and two boreholes for stimulation. The monitoring boreholes are equipped with a multi-modal instrument string including passive seismic sensors, active seismic sources, fiber-optics for distributed sensing, and electrodes for electrical resistivity tomography. Three-dimensional borehole displacements were recorded by two SIMFIP sensors (Guglielmi et al., 2014) deployed in the stimulation and in the production boreholes, respectively.

Here we focus on recordings of the SIMFIP sensor installed in the borehole injection interval and of the passive seismic network only. Results of other monitoring techniques and coupled modelling are described in Kneafsey et al. (2019; 2020; 2021) and references therein. The SIMFIP sensor measures the 3-D displacements of the borehole wall across a pressurized borehole interval using seven Fiber-Bragg gratings (FBG) that sense strain in six different directions of a special-designed cage and pressure. This allows us to infer six degrees of displacement (three translational and three rotational) between two points clamped 0.80 m apart on the borehole wall. The clamped cage sits centered but mechanically decoupled in a 1.64 m long pressurized interval between two inflatable packers. The FBGs were continuously sampled at 1 kHz. The six deformation sensing arms and the pressure sensor of the SIMFIP probe are interrogated with a single ultra-wide wavelength-swept laser which detects the characteristic wavelength of each FBG and its variation with the FBG deformation. Since these 6 strain + 1 pressure data are set on two optical fibers but scanned with the same interrogator, the noise floor is correlated between FBGs. To decrease the relative noise amplitude, we take the pressure channel as reference and apply a zero phase, high-pass Butterworth filter with 25 Hz corner frequency to extract the noise signal. This noise channel, multiplied by a scaling factor to reflect the different noise amplitudes resulting from the sensor geometry, is then subtracted from each of the deformation channels. The results are the deformations without the correlated noise of the interrogator laser. The deformations of the six arms can then be used to calculate the six degrees of freedom of translation and rotation. Seismic activity was recorded by a network of twelve 3-component accelerometers (PCB 356B18) and 24 hydrophones (High Tech HTI-96-Min), continuously sampled at 100 kHz by a 24-bit digitizer (Data Translation, VibBox-64). The sensors were

grouted in place in six monitoring boreholes, surrounding the experimental volume in 3-D (Schoenball et al., 2020).

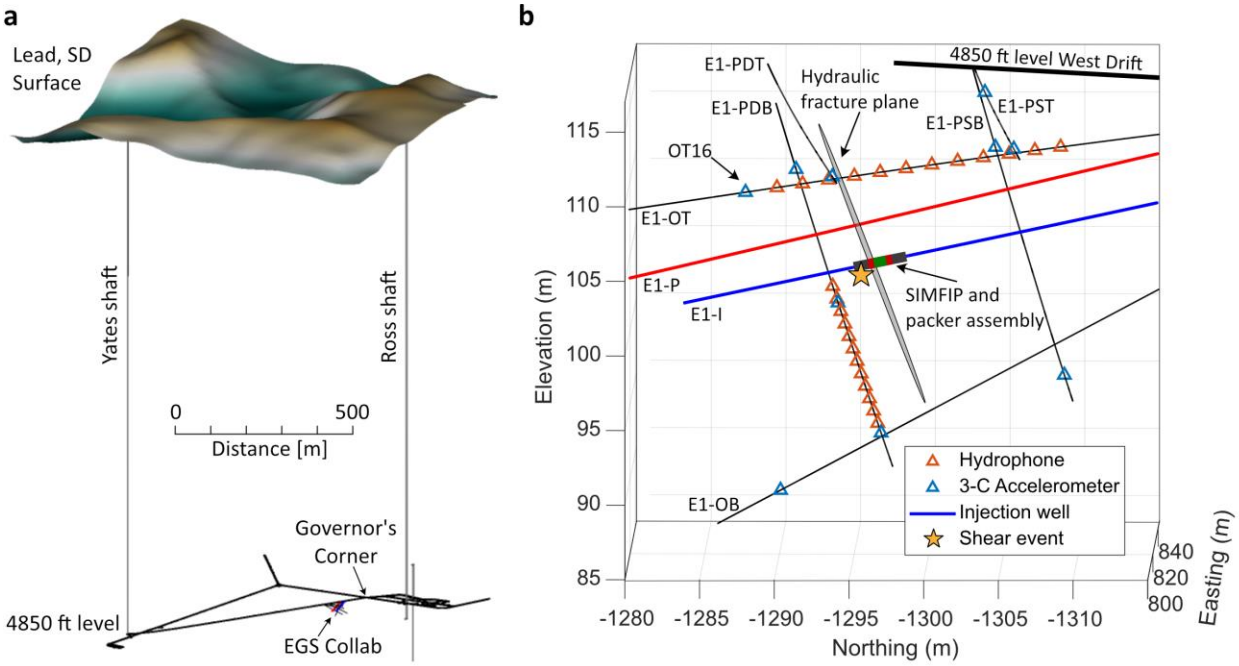


*Figure 1: (a) Location of the EGS Collab testbed on the 4850 ft level at the Sanford Underground Research Facility. (b) Testbed layout with monitoring and experimentation boreholes, and monitoring system. The SIMFIP assembly is drawn to scale and colors correspond to the packers (gray), the pressurized interval (red) and the clamped interval (green). The hydraulic fracture plane determined from event hypocenters is indicated by the gray disk seen almost edge-on. The single shear event (yellow star) was located just below the SIMFIP assembly.*

## Overview of hydraulic testing

The injection borehole was drilled along an azimuth of approximately N358˚E, close to the direction of the least principal stress N002˚E. The hole was drilled with 96 mm diameter and left uncased beyond the first 6 m. The initial injection was performed at approximately 50 m depth. A centimeter-sized notch was cut into the borehole wall to guide the initiation of the hydraulic fracture. Before the experiment, optical (OTV) and acoustic televiewer (ATV) logs were acquired, and a repeat ATV log was acquired after the experiment, which did not reveal significant damage (Figure 2).

The hydraulic test was designed to create a hydraulic fracture of a nominal radius of 1.5 m. The interval was pressurized by a constant injection of 200 mL/min of water. The pore fluid pressure $p$ in the interval rose linearly with time, elastically stressing the interval (Figure S1). Well before the onset of hydraulic fracturing, at 21:55:11 ($p$ = 13.4 MPa) the first seismic event was recorded. This event was accompanied

by significant shear displacements recorded by the SIMFIP probe (Figure 3). We will discuss this event in detail below.

At 21:55:44 UTC ($p$ = 20.9 MPa), the fluid pressure left the linear regime, and displacements indicated the opening of a hydraulic fracture. A first pressure maximum of 24.6 MPa was reached at 21:56:08 UTC (Figure S1). Pressure slowly declined until 21:56:40 UTC ($p$ = 23.5 MPa), when it slowly increased until the end of injection at 22:05:16 UTC ($p$ = 26.3 MPa). The development of the hydraulic fracture during this test and several re-opening and propagation cycles is described in Guglielmi et al. (2021).

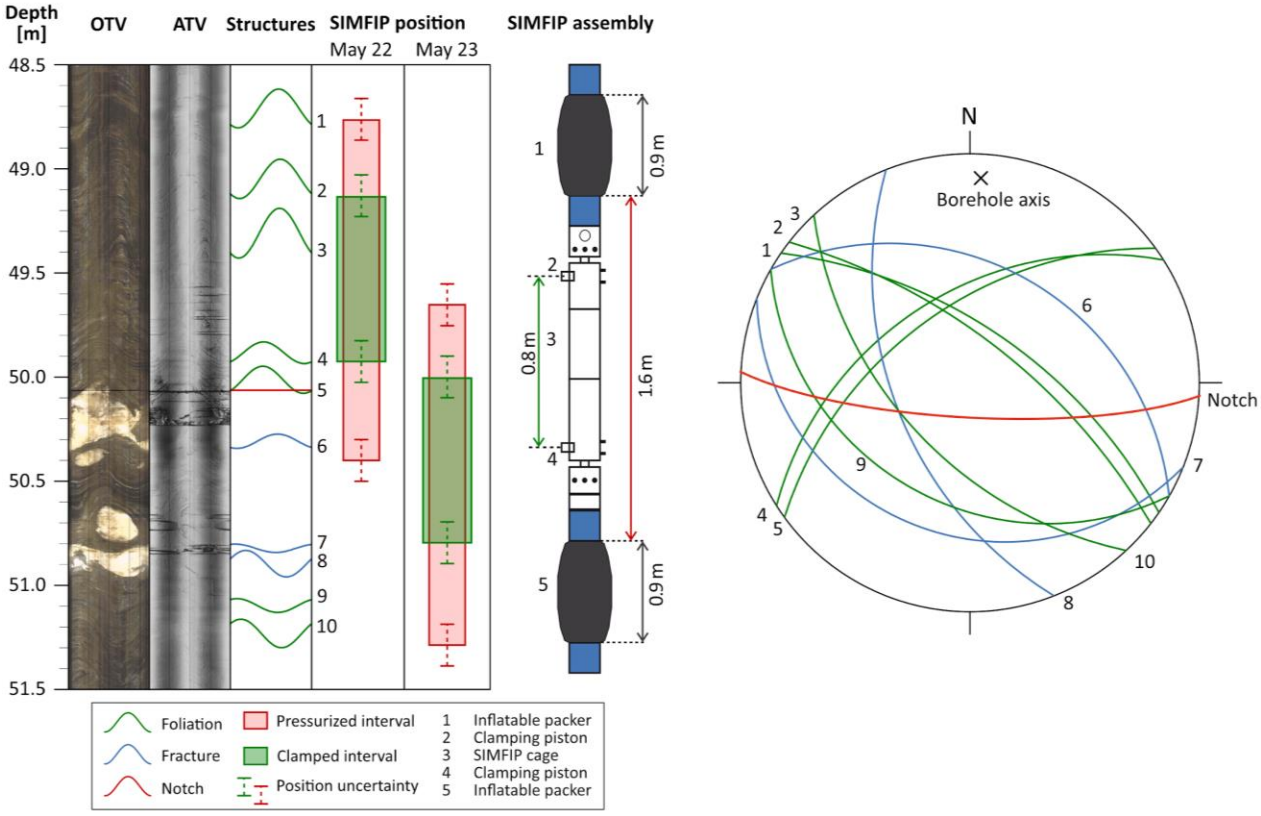


*Figure 2: Optical and acoustic televiewer logs and structural interpretations of the borehole section of E1-I containing the pressurized intervals. The pressurized and clamped intervals on May 22 and May 23 are drawn as red and green rectangles, respectively. The assembly containing the SIMFIP probe and inflatable packers is shown in the middle. On the right, the foliation and fracture planes intersecting the interval are plotted in a lower hemisphere stereo plot. The numbers correspond to the features identified in the Structures panel.*

## Early shear event

Figure 3 shows a close-up of the displacement transient related to the early shear event recorded at 21:55:11 during the injection. Due to technical problems, after each recording interval of about 3 seconds there is a gap of about 2 seconds in the data stream. The fluid pressure measured in the clamped interval was 13.4 MPa and did not show any significant deviation from its linear trend during ongoing pressurization of the packed-off interval. This indicates that no fluid leaked off from the interval as a result of the shear displacement.

We recorded displacements in borehole radial direction during the entire 3-second data segment that includes the event. No displacement was observed during the data segment before. The displacement transient therefore started during the end of a data gap and we just missed the true onset of deformation. From the beginning of the data segment, we observe linearly increasing shear displacements (pre-slip) during about 0.3 s (0.4 s if we extrapolate the linear trend to the beginning) to a total of 7 µm. Shear displacement then continues to increase by 5.5 µm during an accelerated slip event (coseismic) lasting about 0.022 s. Then, displacement decelerates in an exponential-type decay during the remainder of the data segment (afterslip). At the end of the data segment a total of 22 µm of slip had accumulated. Immediately after the coseismic slip, there may be some low frequency reverberations measured by the SIMFIP probe but the signal-to-noise ratio is too small to make a definitive observation.

Based on the 5.5 µm coseismic slip and general scaling relations of earthquakes (Kwiatek et al., 2011), we obtain a slip patch on the order of 1 m and a moment magnitude on the order of $M_W$ −3 to −2.

During the same time period, axial displacements continue to decrease as before during the linear pressure increase. During the slip event, we observe minimal additional axial closure, which confirms that the slippage occurred just outside the clamping interval. Axial deformation during the slip event can be estimated to be less than 1 µm.

At the time of the observed shear displacement, the accelerometer array recorded a seismic event with the strongest waveforms at least until the first pressure maximum was reached at 21:56:08 UTC. It was clearly visible on all channels of the monitoring array. The waveforms (Figure 3b and Figure S2) indicate a complex rupture with at least two sub-events evidenced by two S-wave trains. Manually picked first arrivals of P and S waves were used to locate the event. We determined the hypocenter to be about 0.8 m below the injection interval (Figure 1). Given the formal location uncertainty (2-sigma) of about 1.3 m and that of the borehole trajectory of about 1 m, the event hypocenter could be within the pressurized interval as indicated by the direct measurements of displacement.

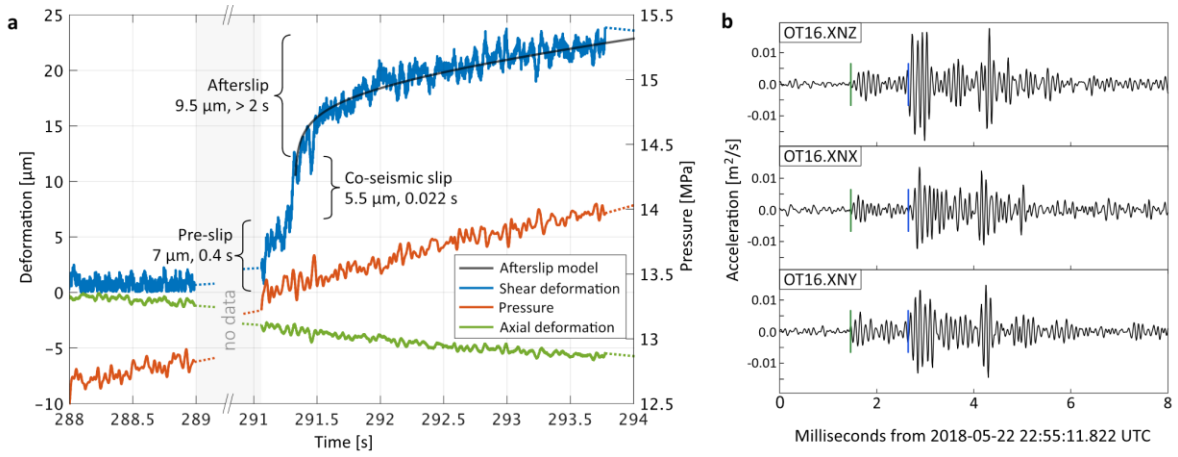


*Figure 3: (a) Shear and axial displacement and injection interval pressure before, during and after the shear event. (b) Seismic waveforms of the shear event at the closest accelerometer OT16, band pass filtered between 3 and 15 kHz. P and S-wave arrivals are marked by green and blue dashes, respectively.*

The goal of this experiment was to create a hydraulic fracture in an intact rock mass. Neither the optical nor the acoustic image logs indicated the presence of fractures within the selected interval for pressurization. However, the phyllite rock mass shows a pervasive fabric with bedding planes of varying orientation. In addition, it contains several quartz inclusions (lighter colored features in the OTV shown in Figure 2).

We did not observe any other discrete shear events in the pressurized interval using the SIMFIP probe during any later test at this location. In other words, although pressure was increasing to much higher levels during the later stages of hydraulic fracturing, there was no repeated activation of the same slip patch. However, additional seismic events could be located close to the injection interval. These were relocated by Chai et al. (2020) using tomoDD for joint inversion for relative locations and a 3-D velocity model. Figure 4 shows the seismicity located during the entire test together with our absolute location of the discrete shear event. We see a clear trend delineated by the hypocenters about 4 m long. We fitted planes to the hypocenters and used bootstrap resampling to evaluate the parameter space of possible planes and computed an average orientation. These, along with the slip vectors measured by the SIMFIP and the structures identified in the image logs, are plotted in Figure 4c. There is good agreement of the possible slip planes and the average plane with foliation planes 1 and 2. Further, the slip vectors also match these planes, indicating that slip initiated on a foliation plane and propagated bi-laterally, as delineated by the later seismic events. The slip vectors also coincide with the plane defined by the machined notch, indicating that it could have helped to initiate the slip event.

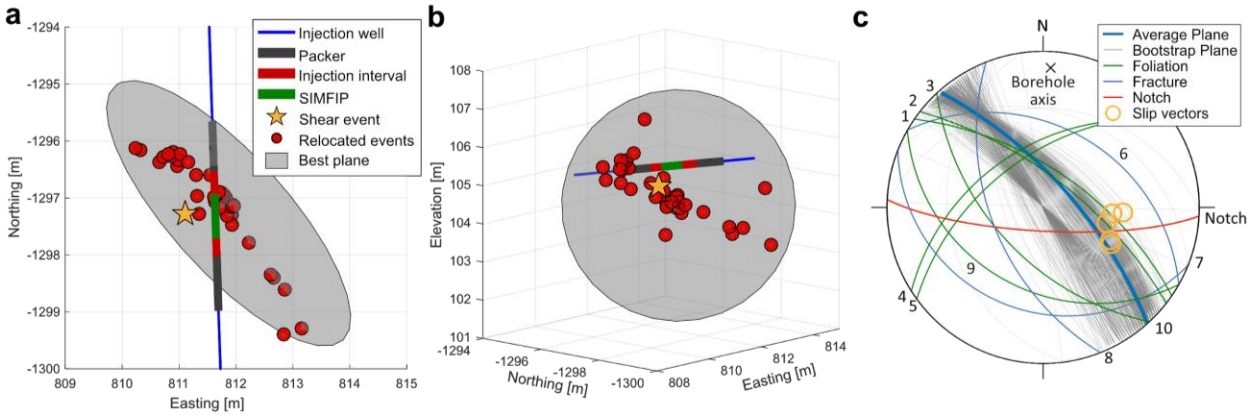


*Figure 4: (a-b) Three-dimensional view of SIMFIP assembly, the absolute location of the shear event and relocated seismicity during the injection step. (c) Stereoplot of structures identified on image logs, possible planes derived from hypocenters of relocated seismicity (Chai et al., 2020) with an average plane and slip vectors for the shear event measured by the SIMFIP*.

## Displacement transients

At the beginning of the data segment we record already about 2 µm displacement that continued to grow linearly. The pre-slip we recorded lasted about 0.3 seconds with a slip speed of about 17.5 µm/s. If we linearly extrapolate the onset of pre-slip into the preceding data gap we estimate the total duration of the pre-slip phase to be about 0.4 s.

Pre-slip transients similar to ours with linearly increasing slip velocity before the transition to dynamic rupture have also been observed by McLaskey & Lockner (2014) in their laboratory experiments on meter-sized samples. Their recorded pre-slips lasted on the order of 10 seconds at slip speeds up to about 0.4 µm/s before they transitioned into unstable dynamic ruptures.

Our spatial and temporal resolution is not sufficient to clearly resolve the co-seismic displacement. At the end of the pre-slip phase, the total displacement jumps by 5.5 µm in 0.022 s. It is likely that the total co-seismic displacement was reached after a much shorter time and the slip velocity was >250 µm/s. The fast coseismic slip transitioned into afterslip with a much lower slip velocity. We model the afterslip using the model proposed in Marone et al. (1991). They provide a closed form solution for the expected afterslip of an earthquake based on rate-and-state friction theory assuming an earthquake that propagates into a velocity-strengthening region and resulting from relaxation of the stress perturbation. It is given by $U_p = \frac{a-b}{k}\, ln\, [(\frac{kV_{CS}}{a-b})t\ +\ 1] + V_0 t$, where $a$-$b$ is the friction rate parameter, $k$ is the thickness-averaged stiffness, $V_0$ is the pre-seismic slip speed, $V_{CS}$ is the thickness-averaged coseismic slip velocity within the velocity strengthening region and $t$ is time. This can be rewritten as

$U_p = \alpha\, ln\, [\frac{V_{CS}}{\alpha} t\ +\ 1]\ + V_0 t$, with $\alpha = \frac{a-b}{k}$. A good fit is achieved for $\alpha = 1.5 \cdot 10^{-6}$ m, $V_{CS} = 2.5 \cdot 10^{-4}$ m/s and $V_0 = 1.2 \cdot 10^{-6}$ m/s (Figure 3a). The pre-seismic slip speed $V_0$ does correspond to the inter-seismic creep measured for fault systems. This value should be negligible in our case since a 13.4 MPa stress change was required to initiate rupture. However, to achieve a good fit during the later period of the afterslip phase, a similar parameter is required. We hypothesize that the continuously increasing pressure (from 13.3 to 14 MPa) during the 3 second slip event may have modulated afterslip and caused this linear component of the deformation transient. Further, we highlight that the recorded displacement transient shares functional behavior with constitutive equations for creep and stress relaxation for bulk rock materials of a wide range of lithologies (Main, 2000; Perfettini & Avouac, 2004; Sone & Zoback, 2013).

We do not see a deviation of the pressure transient from a linear increase during the slip event. Given an upper bound for the crack opening of 5 μm and a fracture area of 1 $m^2$, an additional volume of up to 5 μL could have been created. In the 3 second time frame of the slip event, the fluid increment from the ongoing injection was 10 mL, which is much larger than what could possibly leak-off into the reactivated fracture. Hence the measured injection pressure could not have been perturbed by the slip event.

## Conclusions

Before opening a hydraulic fracture, we observed shear reactivation of a preexisting weakness associated with a seismic event. The obtained location and activation pressure are consistent with slip on a foliation plane. Additional pressurization in the first and subsequent injections could not reactivate this slip patch further. No other episodic displacements were measured that could be tied to discrete events.

For the first time, we directly observed co-seismic deformation including the three phases of shear slip that were previously only observed separately or were only predicted by numerical models. Of the total accumulated slip about 30% occurred as pre-slip, 25% occurred co-seismically, leading to recorded seismic waves, and 45% occurred as transient afterslip. The observed pre-slip demonstrates stable sliding conditions leading into fast co-seismic slip. Slip was arrested over a three second period of afterslip. No further reactivation of this fracture was observed later when hydraulic fracturing conditions were achieved, indicating a total stress drop of the slip patch.

The activated orientation is also very active in later stimulations as shown in Schoenball et al. (2020). This indicates that rock fabric such as bedding and foliation planes may play a bigger role in hydraulic stimulations than previously thought.

## Appendix 1: EGS Collab Team

J. Ajo-Franklin[1,2], T. Baumgartner[3], K. Beckers[4], D. Blankenship[5], A. Bonneville[6], L. Boyd[7], S. Brown[8], J.A. Burghardt[6], C. Chai[9], A. Chakravarty[1], T. Chen[10], Y. Chen[10], B. Chi[2], K. Condon[11], P.J. Cook[1], D. Crandall[8], P.F. Dobson[1], T. Doe[12], C.A. Doughty[1], D. Elsworth[13], J. Feldman[5], Z. Feng[10], A. Foris[5], L.P. Frash[10], Z. Frone[7], P. Fu[14], K. Gao[10], A. Ghassemi[15], Y. Guglielmi[1], B. Haimson[11], A. Hawkins[16], J. Heise[3], C. Hopp[1], M. Horn[3], R.N. Horne[16], J. Horner[6], M. Hu[1], H. Huang[17], L. Huang[10], K.J. Im[13], M. Ingraham[5], E. Jafarov[10], R.S. Jayne[1], T.C. Johnson[6], S.E. Johnson[1], B. Johnston[4], S. Karra[10], K. Kim[1], D.K. King[5], T. Kneafsey[1], H. Knox[6], J. Knox[6], D. Kumar[15], K. Kutun[18], M. Lee[5], K. Li[16], Z. Li[13], M. Maceira[9], P. Mackey[8], N. Makedonska[10], C.J. Marone[13], E. Mattson[19], M.W. McClure[20], J. McLennan[21], T. McLing[17], C. Medler[22], R.J. Mellors[14], E. Metcalfe[7], J. Miskimins[18], J. Moore[8], C.E. Morency[14], J.P. Morris[14], T. Myers[5], S. Nakagawa[1], G. Neupane[17], G. Newman[1], A. Nieto[7], T. Paronish[8], R. Pawar[10], P. Petrov[1], B. Pietzyk[3], R. Podgorney[17], Y. Polsky[9], J. Pope[5], S. Porse[7], J.C. Primo[1], C. Reimers[22], B.Q. Roberts[6], M. Robertson[1], V. Rodriguez-Tribaldos[1], W. Roggenthen[22], J. Rutqvist[1], D. Rynders[3], M. Schoenball[1], P. Schwering[5], V. Sesetty[15], C.S. Sherman[14], A. Singh[16], M.M. Smith[14], H. Sone[11], E.L. Sonnenthal[1], F.A. Soom[1], D.P. Sprinkle[6], S. Sprinkle[1], C.E. Strickland[6], J. Su[5], D. Templeton[14], J.N. Thomle[6], C. Ulrich[1], N. Uzunlar[22], A. Vachaparampil[15], C.A. Valladao[1], W. Vandermeer[7], G. Vandine[3], D. Vardiman[3], V.R. Vermeul[6], J.L. Wagoner[14], H.F. Wang[11], J. Weers[4], N. Welch[10], J. White, M.D. White[6], P. Winterfeld[18], T. Wood[1], S. Workman[8], H. Wu[14], Y.S. Wu[18], E.C. Yildirim[13], Y. Zhang[16], Y.Q. Zhang[1], Q. Zhou[1], M.D. Zoback[16]

[1] Lawrence Berkeley National Laboratory, [2] Rice University, [3] Sanford Underground Research Facility, [4] National Renewable Energy Laboratory, [5] Sandia National Laboratories, [6] Pacific Northwest National Laboratory, [7] U.S. Department of Energy, [8] National Energy Technology Laboratory, [9] Oak Ridge National Laboratory, [10] Los Alamos National Laboratory, [11] University of Wisconsin-Madison, [12] TDoeGeo Rock Fracture Consulting; Golder Associates Inc, [13] Pennsylvania State University, [14] Lawrence Livermore National Laboratory, [15] The University of Oklahoma, [16] Stanford University, [17] Idaho National Laboratory, [18] Colorado School of Mines, [19] Mattson Hydrology LLC, [20] ResFrac, [21] University of Utah, [22] South Dakota School of Mines and Technology

## Acknowledgements

We thank Eric Dunham for helpful discussions. This material was based upon work supported by the U.S. Department of Energy, Office of Energy Efficiency and Renewable Energy (EERE), Office of Technology Development, Geothermal Technologies Office, under Award Number DE-AC02-05CH11231 with LBNL. The United States Government retains, and the publisher, by accepting the

article for publication, acknowledges that the United States Government retains a non-exclusive, paid-up, irrevocable, world-wide license to publish or reproduce the published form of this manuscript, or allow others to do so, for United States Government purposes. The research supporting this work took place in whole or in part at the Sanford Underground Research Facility in Lead, South Dakota. The assistance of the Sanford Underground Research Facility and its personnel in providing physical access and general logistical and technical support is acknowledged.

## Data Availability Statement

The data presented in this manuscript can be accessed from the Geothermal Data Repository at https://gdr.openei.org/submissions/1289.

## References

Cattania, C., & Segall, P. (2020). Precursory slow slip and foreshocks on rough faults. *EarthArXiv Preprints*, doi:10.31223/osf.io/9xphk

Chai, C., Maceira, M., Santos-Villalobos, H.J., Venkatakrishnan, S.V., Schoenball, M., Zhu, W., Beroza, G.C., Thurber, C., EGS Collab Team (2020). Using a Deep Neural Network and Transfer Learning to Bridge Scales for Seismic Phase Picking. *Geophys. Res. Lett.*, doi:10.1029/2020GL088651

Ellsworth, W. L., & Beroza, G. C. (1995). Seismic Evidence for an Earthquake Nucleation Phase. *Science*, *268*(5212), 851–855. https://doi.org/10.1126/science.268.5212.851

Ellsworth, W. L., & Bulut, F. (2018). Nucleation of the 1999 Izmit earthquake by a triggered cascade of foreshocks. *Nature Geoscience*, *11*(7), 531–535. https://doi.org/10.1038/s41561-018-0145-1

Heise, J. (2015). The Sanford Underground Research Facility at Homestake. Journal of Physics: Conference Series, v. 606 (1), *IOP Publishing*, 25 p., doi:10.1088/1742-6596/606/1/012015

Guglielmi, Y., Cappa, F., Lançon, H., Janowcsyk, J. B., Rutqvist, J., Tsang, C.-F., & Wang, J. S. Y. (2014). ISRM Suggested Method for Step-Rate Injection Method for Fracture In-Situ Properties (SIMFIP): Using a 3-Components Borehole Deformation Sensor. *Rock Mechanics and Rock Engineering*, *47*(1), 303–311. https://doi.org/10.1007/s00603-013-0517-1

Guglielmi, Y., Cook, P., Soom, F., Schoenball, M., Dobson, P., & Kneafsey, T. (2021). In situ continuous monitoring of borehole displacements induced by stimulated hydrofracture growth. *Geophysical Research Letters*, 48, e2020GL090782. https://doi.org/10.1029/2020GL090782

Kneafsey, T. J., Blankenship, D., Knox, H. A., Johnson, T. C., Ajo-Franklin, J. B., Schwering, P. C., et al. (2019). EGS Collab Project: Status and Progress. In *Proceedings 44th Workshop on Geothermal Reservoir Engineering*, *Stanford University*, 16 p.

Kneafsey, T. J., Blankenship, D., Dobson, P. F., Morris, J. P., White, M. D., Fu, P., et al. (2020). The EGS Collab Project: Learnings from Experiment 1. In *Proceedings 45th Workshop on Geothermal Reservoir Engineering*, 15 p., Stanford University, Stanford, California.

Kneafsey, T., Blankenship, D., Dobson, P., White, M., Morris, J.P., Fu, P., Wu, H., Schwering, P.C., et al. (2021). Fracture stimulation and chilled-water circulation through deep crystalline rock: Characterization, modeling, monitoring, and heat-transfer assessment. In *Proceedings, 46th Workshop on Geothermal Reservoir Engineering*, Stanford University, Stanford, California.

Kwiatek, G., Plenkers, K., Dresen, G., JAGUARS Research Group (2011) Source Parameters of Picoseismicity Recorded at Mponeng Deep Gold Mine, South Africa: Implications for Scaling Relations. *Bulletin of the Seismological Society of America*; 101 (6): 2592–2608. doi: https://doi.org/10.1785/0120110094

Main, I. G. (2000). A damage mechanics model for power-law creep and earthquake aftershock and foreshock sequences. *Geophysical Journal International*, 142(1), 151–161. https://doi.org/10.1046/j.1365-246x.2000.00136.x

Marone, C. J., Scholtz, C. H., & Bilham, R. (1991). On the mechanics of earthquake afterslip. *Journal of Geophysical Research*, 96(B5), 8441. https://doi.org/10.1029/91JB00275

McLaskey, G. C., & Lockner, D. A. (2014). Preslip and cascade processes initiating laboratory stick slip. *Journal of Geophysical Research: Solid Earth*, 119(8), 6323–6336. https://doi.org/10.1002/2014JB011220

McLaskey, G. C. (2019). Earthquake Initiation from Laboratory Observations and Implications for Foreshocks. *Journal of Geophysical Research: Solid Earth*, 124(12), 12882–12904. https://doi.org/10.1029/2019JB018363

McGuire, J. J., Boettcher, M. S., & Jordan, T. H. (2005). Foreshock sequences and short-term earthquake predictability on East Pacific Rise transform faults. *Nature*, 434(7032), 457–461. https://doi.org/10.1038/nature03377

Nadeau, R. M., & Johnson, L. R. (1998). Seismological studies at Parkfield VI: Moment release rates and estimates of source parameters for small repeating earthquakes. *Bulletin of the Seismological Society of America*, 88(3), 790–814.

Perfettini, H., & Avouac, J.-P. (2004). Postseismic relaxation driven by brittle creep: A possible mechanism to reconcile geodetic measurements and the decay rate of aftershocks, application to the Chi-Chi earthquake, Taiwan. *Journal of Geophysical Research: Solid Earth*, 109(B2). https://doi.org/10.1029/2003JB002488

Savage, H. M., Kirkpatrick, J. D., Mori, J. J., Brodsky, E. E., Ellsworth, W. L., Carpenter, B. M., et al. (2017). Scientific Exploration of Induced SeisMicity and Stress (SEISMS). *Scientific Drilling*, 23, 57–63. https://doi.org/10.5194/sd-23-57-2017

Schoenball, M., Baujard, C., Kohl, T., & Dorbath, L. (2012). The role of triggering by static stress transfer during geothermal reservoir stimulation. *Journal of Geophysical Research*, 117(B9), B09307. https://doi.org/10.1029/2012jb009304

Schoenball, M., Ajo-Franklin, J. B., Blankenship, D., Chai, C., Chakravarty, A., Dobson, P., et al. (2020). Creation of a mixed-mode fracture network at mesoscale through hydraulic fracturing and shear stimulation. *Journal of Geophysical Research: Solid Earth*, 125, e2020JB019807. https://doi.org/10.1029/2020JB019807

Sone, H., & Zoback, M. D. (2013). Mechanical properties of shale-gas reservoir rocks — Part 2: Ductile creep, brittle strength, and their relation to the elastic modulus. *GEOPHYSICS*, 78(5), D393–D402. https://doi.org/10.1190/geo2013-0051.1

Tape, C., Holtkamp, S., Silwal, V., Hawthorne, J., Kaneko, Y., Ampuero, J. P., et al. (2018). Earthquake nucleation and fault slip complexity in the lower crust of central Alaska. *Nature Geoscience*, *11*(7), 536–541. https://doi.org/10.1038/s41561-018-0144-2

Yoon, C. E., Yoshimitsu, N., Ellsworth, W. L., & Beroza, G. C. (2019). Foreshocks and Mainshock Nucleation of the 1999 M w 7.1 Hector Mine, California, Earthquake. *Journal of Geophysical Research: Solid Earth*, *124*(2), 1569–1582. doi:10.1029/2018JB016383